Huntley, S., Jones, D., & Gaitonde, A. (2017). Aeroelastic Gust Response of an Aircraft Using a Prescribed Velocity Method in Viscous Flows. In 23rd AIAA Computational Fluid Dynamics Conference. [AIAA 2017-3616] American Institute of Aeronautics and Astronautics Inc, AIAA. DOI: 10.2514/6.2017-3616

Aeroelastic Gust Response of an Aircraft Using a Prescribed Velocity Method in Viscous Flows

S. J. Huntley*, D. Jones† and A. Gaitonde†

Department of Aerospace Engineering, University of Bristol, Bristol, BS8 1TR, United Kingdom

This paper presents the extension of the prescribed velocity method, known as the Split Velocity Method, for the purposes of modelling flexible aircraft gust responses. This is achieved by performing aeroelastic simulations using the computational fluid dynamics flow solver DLR-TAU coupled with a modal structural solver. This method is demonstrated by computing the response of a wide-body aircraft to a series of 1-cosine gusts. The results are compared to an existing prescribed velocity method, the Field Velocity Method. It is shown that the Field Velocity Method is a simplification of the Split Velocity Method and this results in noticeable differences in the solution for short wavelength gusts, where the velocity gradients are greatest.

Nomenclature

$\hat{\hat{u}}, \hat{\hat{v}}, \hat{\hat{w}}$	gust velocity components
γ	ratio of specific heats
μ	dynamic viscosity
ρ	density
$\tilde{u}, \tilde{v}, \tilde{w}$	background velocity components
c	chord length
E	energy
p	pressure
Pr	Prandtl number
Re	Reynolds number
s	non-dimensional time
t	time
u, v, w	total velocity components
u_{ref}	freestream velocity
x_t, y_t, z_t	grid velocities

I. Introduction

Previous work by the authors demonstrated the applicability of the Split Velocity Method (SVM) to improve the prediction of the rigid gust response of aircraft.[1] This paper extends that work to flexible gust responses by including a structural solver and deformation tool in the solution process to perform an aeroelastic gust analysis.

As an aircraft encounters a gust it undergoes a large change in the loads and moments it experiences. This in turn changes the shape of the aircraft as it responds to these forces. As the gust constitutes a critical load case in the design of the aircraft, its accurate prediction is important for safety and certification. Inclusion of the aeroelastic effects becomes important as the flexible dynamic response of the aircraft, that is excited by the gust, impact on the structural design and fatigue calculations.

*Research Associate, AIAA member

†Senior Aerodynamics Lecturer, AIAA member

During the detailed design stages, high fidelity solutions are required. This is achieved using Computational Fluid Dynamics (CFD). CFD simulations are associated with high computational cost, which is especially true for unsteady applications, such as is of interest in this work. Furthermore, the accuracy achievable in CFD is limited by numerical dissipation.[2] Numerical dissipation is most prevalent in spatial regions where the grid is not resolved enough. In these regions any disturbances, such as gusts and vortices, are quickly diffused.[3] This is often the case in the far field upstream regions. This can be overcome by using a mesh which is fine throughout the domain, however this significantly increases the computational cost and as such becomes an impractical solution for design purposes. An alternative to using a globally fine mesh is to locally adapt the mesh so that the resolution is fine enough in the spatial regions of interest.[4] Once again, this increases the computational cost as a grid generator must be employed whilst the simulation is performed. Furthermore, this method is not guaranteed to result in more accurate results as the grid can become distorted, thus reducing its quality.[5]

The problem of needing to employ a fine mesh throughout the domain can be overcome by using a prescribed velocity method. Prescribed velocity methods work by prescribing the disturbance velocities, in this case the gust velocities, and changing the grid time metrics. In this way grid motion is simulated but the mesh is not altered or distorted.[6,7] This is the approach taken in the Field Velocity Method (FVM).[8] Here, the concept of the surface transpiration method has been taken and extended so that velocity corrections are not just applied on the surface but are applied throughout the flow domain.[9] Numerical dissipation of the gust disturbance is eliminated as the gust velocities are prescribed, which means that the computational cost can be reduced as a coarser mesh can be used away from the aircraft. One further benefit to this method is the fact that it is easily implemented as it reuses existing moving mesh Euler or Navier-Stokes codes by setting the grid velocities to the negative of the gust velocities. In the literature, FVM has been used in a range of applications from solving sharp edged gusts[7] to modelling a step change in flow incidence[6] and for vortex interaction problems.[10] It has also been validated by analytical solutions from piston and linear compressible theories.[6] However, FVM is not appropriate for modelling certain downstream problems, such as a horizontal stabilizer as it does not include all the interactions between the aircraft and the gust, it only accounts for the influence of the gust on the aircraft.[11] The available literature for FVM does not make clear what the underlying assumptions are and furthermore does not appear to consider the momentum and energy components due to the external velocity field.[9] The Split Velocity Method (SVM) also prescribes gust velocities but, unlike FVM, it retains all momentum and energy components. This is done by rearranging the unsteady governing equations on a fixed or moving mesh. The result of this is more accurate solutions due to the inclusion of some additional source terms, which account for all the interactions between the gust and the aircraft, which will be shown to be missing from FVM. The SVM has been applied to the simulation of gusts in two-dimensional inviscid flows[12] and two- and three-dimensional viscous flow.[1] This study aims to extend the three-dimensional viscous work, which was concerned with the rigid response, by coupling a CFD solver employing SVM to a Computational Structural Mechanics (CSM) solver in order to investigate the aeroelastic gust response of an aircraft. Simulations are carried out for a series of 1-cosine gusts and the solutions are compared to those produced using FVM. The results corroborate those found in Huntley *et. al*,[1] where the results using SVM are more accurate than FVM, especially for short wavelength gusts.

II. Methodology

Aeroelastic simulations involve coupling Computational Fluid Dynamics with Computational Structural Mechanics (CFD-CSM) to get the required aerodynamic coefficients, dimensional forces and moments along the three body axes. This work uses the CFD solver DLR-TAU coupled to a modal CSM solver written in Python. The coupling is performed through the common interface environment provided by FlowSimulator.[13] First the formulation of CFD modelling of gusts using the two prescribed velocity methods used in this work is presented before the coupling to the structural solver is described.

II.A. CFD Modelling of gusts using prescribed velocity methods

The FVM and SVM are both prescribed velocity methods. Both use a moving mesh solver, however, the SVM requires additional source terms. It is possible to formulate the SVM in such a way that it can be shown that the FVM is a simplification of the SVM and that the source terms arising from rearranging the governing equations are neglected. The flow equations may then be solved in conjunction with a structural

solver to compute a flexible aircraft gust encounter or alone for a rigid aircraft gust encounter.

II.A.1. Field Velocity Method

The current method for simulating the gust response of aircraft in DLR-TAU uses a method known as the Field Velocity Method (FVM). In FVM, the gust velocity is prescribed and the remaining flow field is solved; this eliminates numerical dissipation of the disturbances. This allows for coarser meshes to be used away from the aircraft thus significantly reducing computational cost. This method is also cost efficient since it is based on existing moving mesh codes which are easily modified with grid velocities set to minus the gust velocities. In this way, the grid is not actually moved and then the velocities that are computed are relative to the gust. In other words, FVM treats the problem as if the aircraft was moving at the speed of the gust but in the opposite direction. The main drawback of FVM is that it does not include all the interactions between the gust and the aircraft. This has the largest effect on the downstream components and short gusts. The FVM formulation for the Navier-Stokes equations on a fixed mesh in three dimensions are given by Eq. (1).

$$\frac{\partial}{\partial t}\begin{bmatrix}\rho\\ \rho\tilde{u}\\ \rho\tilde{v}\\ \rho\tilde{w}\\ \rho E\end{bmatrix}+\frac{\partial}{\partial x}\begin{bmatrix}\rho(\tilde{u}-x_t)\\ \rho\tilde{u}(\tilde{u}-x_t)+p\\ \rho\tilde{v}(\tilde{u}-x_t)\\ \rho\tilde{w}(\tilde{u}-x_t)\\ \rho E(\tilde{u}-x_t)+p\tilde{u}\end{bmatrix}+\frac{\partial}{\partial y}\begin{bmatrix}\rho(\tilde{v}-y_t)\\ \rho\tilde{u}(\tilde{v}-y_t)\\ \rho\tilde{v}(\tilde{v}-y_t)+p\\ \rho\tilde{w}(\tilde{v}-y_t)\\ \rho E(\tilde{v}-y_t)+p\tilde{v}\end{bmatrix}+\frac{\partial}{\partial z}\begin{bmatrix}\rho(\tilde{w}-z_t)\\ \rho\tilde{u}(\tilde{w}-z_t)\\ \rho\tilde{v}(\tilde{w}-z_t)\\ \rho\tilde{w}(\tilde{w}-z_t)+p\\ \rho E(\tilde{w}-z_t)+p\tilde{w}\end{bmatrix}$$
$$+\frac{\partial}{\partial x}\begin{bmatrix}0\\ \tilde{\sigma}_{xx}\\ \tilde{\sigma}_{xy}\\ \tilde{\sigma}_{xz}\\ \tilde{u}\tilde{\sigma}_{xx}+\tilde{v}\tilde{\sigma}_{xy}+\tilde{w}\tilde{\sigma}_{xz}+q_x\end{bmatrix}+\frac{\partial}{\partial y}\begin{bmatrix}0\\ \tilde{\sigma}_{xy}\\ \tilde{\sigma}_{yy}\\ \tilde{\sigma}_{yz}\\ \tilde{u}\tilde{\sigma}_{xy}+\tilde{v}\tilde{\sigma}_{yy}+\tilde{w}\tilde{\sigma}_{yz}+q_y\end{bmatrix}+\frac{\partial}{\partial z}\begin{bmatrix}0\\ \tilde{\sigma}_{xz}\\ \tilde{\sigma}_{yz}\\ \tilde{\sigma}_{zz}\\ \tilde{u}\tilde{\sigma}_{xz}+\tilde{v}\tilde{\sigma}_{yz}+\tilde{w}\tilde{\sigma}_{zz}+q_z\end{bmatrix}=0 \tag{1}$$

Where the equations are actually the moving mesh equations with the grid velocities set equal to the negative gust velocities

$$x_t=-\hat{\tilde{u}},\quad y_t=-\hat{\tilde{v}},\quad z_t=-\hat{\tilde{w}} \tag{2}$$

The energy and pressure are given by

$$E=\frac{p}{\rho(\gamma-1)}+\frac{1}{2}(\tilde{u}^2+\tilde{v}^2+\tilde{w}^2) \tag{3}$$

and

$$p=(\gamma-1)(\rho E-\frac{\rho}{2}(\tilde{u}^2+\tilde{v}^2+\tilde{w}^2)) \tag{4}$$

respectively.

The FVM has been shown to yield accurate results for very thin aerofoils by comparing with exact flat-plate analytical solutions from piston theory and linear steady state values.[6] However, FVM is not backed by any compelling reason or clear description of simplifications and assumptions used in its derivation.

II.A.2. Split Velocity Method

The Split Velocity Method (SVM) is another method which prescribes the gust velocities but retains all momentum and energy components. This is achieved by decomposing the velocities and energy in the unsteady governing equations before rearranging them. There are no simplifications or assumptions made in the formulation of the SVM from the Navier-Stokes equations and the formulation presented here can be compared directly to the FVM. This makes it clear that the FVM neglects additional source terms which are present in SVM. These source terms account for influence of the aircraft on the gust, which the FVM cannot model,[14] and therefore provides more accurate solutions when this influence is significant. This is especially

true for short gusts due to the effect of spatial gradients in the source terms. For the Split Velocity Method, the formulation begins with the unsteady Navier-Stokes equations on a fixed mesh (Eq. (5))

$$\begin{aligned}
&\frac{\partial}{\partial t}\begin{bmatrix}\rho\\ \rho u\\ \rho v\\ \rho w\\ \rho E\end{bmatrix}+\frac{\partial}{\partial x}\begin{bmatrix}\rho u\\ \rho u^2+p\\ \rho uv\\ \rho uw\\ u(\rho E+p)\end{bmatrix}+\frac{\partial}{\partial y}\begin{bmatrix}\rho v\\ \rho vu\\ \rho v^2+p\\ \rho vw\\ v(\rho E+p)\end{bmatrix}\\
&+\frac{\partial}{\partial z}\begin{bmatrix}\rho w\\ \rho wu\\ \rho wv\\ \rho w^2+p\\ w(\rho E+p)\end{bmatrix}+\frac{\partial}{\partial x}\begin{bmatrix}0\\ \sigma_{xx}\\ \sigma_{xy}\\ \sigma_{xz}\\ u\sigma_{xx}+v\sigma_{xy}+w\sigma_{xz}+q_x\end{bmatrix}\\
&+\frac{\partial}{\partial y}\begin{bmatrix}0\\ \sigma_{xy}\\ \sigma_{yy}\\ \sigma_{zy}\\ u\sigma_{xy}+v\sigma_{yy}+w\sigma_{yz}+q_y\end{bmatrix}+\frac{\partial}{\partial z}\begin{bmatrix}0\\ \sigma_{xz}\\ \sigma_{yz}\\ \sigma_{zz}\\ u\sigma_{xz}+v\sigma_{yz}+w\sigma_{zz}+q_z\end{bmatrix}=0
\end{aligned}\tag{5}$$

and decomposes the velocities and energy as

$$u=\tilde{u}+\hat{\hat{u}}\qquad v=\tilde{v}+\hat{\hat{v}}\qquad w=\tilde{w}+\hat{\hat{w}}\qquad E=\tilde{E}+\hat{\tilde{E}}+\hat{\hat{E}}\tag{6}$$

where $\hat{\hat{u}}$, $\hat{\hat{v}}$ and $\hat{\hat{w}}$ are the gust velocity components. The Energy, E, is computed by substituting the velocity decompositions into Eq. (3), which after some manipulation gives

$$E=\underbrace{\frac{p}{\rho(\gamma-1)}+\frac{1}{2}(\tilde{u}^2+\tilde{v}^2+\tilde{w}^2)}_{\tilde{E}}+\underbrace{(\tilde{u}\hat{\hat{u}}+\tilde{v}\hat{\hat{v}}+\tilde{w}\hat{\hat{w}})}_{\hat{\tilde{E}}}+\underbrace{\frac{1}{2}(\hat{\hat{u}}^2+\hat{\hat{v}}^2+\hat{\hat{w}}^2)}_{\hat{\hat{E}}}\tag{7}$$

The pressure remains unchanged from the FVM formulation and is therefore given by Eq. (4). The Navier-Stokes equations for the Split Velocity Method are then obtained by substituting the decompositions in Eq. (6) into the unsteady Navier-stokes equations given by Eq. (5).

which, after some manipulation gives the Navier-Stokes equations as

$$\begin{aligned}
&\frac{\partial}{\partial t}\begin{bmatrix}\rho\\ \rho\tilde{u}\\ \rho\tilde{v}\\ \rho\tilde{w}\\ \rho\tilde{E}\end{bmatrix}+\frac{\partial}{\partial x}\begin{bmatrix}\rho(\tilde{u}+\hat{\hat{u}})\\ \rho\tilde{u}(\tilde{u}+\hat{\hat{u}})+p\\ \rho\tilde{v}(\tilde{u}+\hat{\hat{u}})\\ \rho\tilde{w}(\tilde{u}+\hat{\hat{u}})\\ \rho\tilde{E}(\tilde{u}+\hat{\hat{u}})+p\tilde{u}\end{bmatrix}+\frac{\partial}{\partial y}\begin{bmatrix}\rho(\tilde{v}+\hat{\hat{v}})\\ \rho\tilde{u}(\tilde{v}+\hat{\hat{v}})\\ \rho\tilde{v}(\tilde{v}+\hat{\hat{v}})+p\\ \rho\tilde{w}(\tilde{v}+\hat{\hat{v}})\\ \rho\tilde{E}(\tilde{v}+\hat{\hat{v}})+p\tilde{v}\end{bmatrix}+\frac{\partial}{\partial z}\begin{bmatrix}\rho(\tilde{w}+\hat{\hat{w}})\\ \rho\tilde{u}(\tilde{w}+\hat{\hat{w}})\\ \rho\tilde{v}(\tilde{w}+\hat{\hat{w}})\\ \rho\tilde{w}(\tilde{w}+\hat{\hat{w}})+p\\ \rho\tilde{E}(\tilde{w}+\hat{\hat{w}})+p\tilde{w}\end{bmatrix}\\
&+\frac{\partial}{\partial x}\begin{bmatrix}0\\ \sigma_{xx}\\ \sigma_{xy}\\ \sigma_{xz}\\ \tilde{u}\sigma_{xx}+\tilde{v}\sigma_{xy}+\tilde{w}\sigma_{xz}+q_x\end{bmatrix}+\frac{\partial}{\partial y}\begin{bmatrix}0\\ \sigma_{xy}\\ \sigma_{yy}\\ \sigma_{yz}\\ \tilde{u}\sigma_{xy}+\tilde{v}\sigma_{yy}+\tilde{w}\sigma_{yz}+q_y\end{bmatrix}\\
&+\frac{\partial}{\partial z}\begin{bmatrix}0\\ \sigma_{xz}\\ \sigma_{yz}\\ \sigma_{zz}\\ \tilde{u}\sigma_{xz}+\tilde{v}\sigma_{yz}+\tilde{w}\sigma_{zz}+q_z\end{bmatrix}+\begin{bmatrix}0\\ s_m(\hat{\hat{u}})\\ s_m(\hat{\hat{v}})\\ s_m(\hat{\hat{w}})\\ s_e(\hat{\hat{u}},\hat{\hat{v}},\hat{\hat{w}})\end{bmatrix}=0.
\end{aligned}\tag{8}$$

where,

$$\sigma_{xx}=\tfrac{2}{3}\tfrac{\mu}{Re}\left(2\tfrac{\partial\tilde{u}}{\partial x}-\tfrac{\partial\tilde{v}}{\partial y}-\tfrac{\partial\tilde{w}}{\partial z}\right)+\tfrac{2}{3}\tfrac{\mu}{Re}\left(2\tfrac{\partial\hat{\hat{u}}}{\partial x}-\tfrac{\partial\hat{\hat{v}}}{\partial y}-\tfrac{\partial\hat{\hat{w}}}{\partial z}\right)\quad\sigma_{yy}=\tfrac{2}{3}\tfrac{\mu}{Re}\left(2\tfrac{\partial\tilde{v}}{\partial y}-\tfrac{\partial\tilde{u}}{\partial x}-\tfrac{\partial\tilde{w}}{\partial z}\right)+\tfrac{2}{3}\tfrac{\mu}{Re}\left(2\tfrac{\partial\hat{\hat{v}}}{\partial y}-\tfrac{\partial\hat{\hat{u}}}{\partial x}-\tfrac{\partial\hat{\hat{w}}}{\partial z}\right)$$

$$\sigma_{zz} = \frac{2}{3}\frac{\mu}{Re}\left(2\frac{\partial\tilde{w}}{\partial z} - \frac{\partial\tilde{v}}{\partial y} - \frac{\partial\tilde{u}}{\partial x}\right) + \frac{2}{3}\frac{\mu}{Re}\left(2\frac{\partial\hat{w}}{\partial z} - \frac{\partial\hat{v}}{\partial y} - \frac{\partial\hat{u}}{\partial x}\right) \quad \sigma_{xy} = \frac{\mu}{Re}\left(\frac{\partial\tilde{u}}{\partial y} + \frac{\partial\tilde{v}}{\partial x}\right) + \frac{\mu}{Re}\left(\frac{\partial\hat{u}}{\partial y} + \frac{\partial\hat{v}}{\partial x}\right)$$

$$\sigma_{xz} = \frac{\mu}{Re}\left(\frac{\partial\tilde{u}}{\partial z} + \frac{\partial\tilde{w}}{\partial x}\right) + \frac{\mu}{Re}\left(\frac{\partial\hat{u}}{\partial z} + \frac{\partial\hat{w}}{\partial x}\right) \quad \sigma_{yz} = \frac{\mu}{Re}\left(\frac{\partial\tilde{v}}{\partial z} + \frac{\partial\tilde{w}}{\partial y}\right) + \frac{\mu}{Re}\left(\frac{\partial\hat{v}}{\partial z} + \frac{\partial\hat{w}}{\partial y}\right)$$

$$q_x = -\frac{\mu}{Pr}\frac{1}{Re}\frac{1}{(\gamma-1)M_\infty^2}\frac{\partial T}{\partial x} \quad q_y = -\frac{\mu}{Pr}\frac{1}{Re}\frac{1}{(\gamma-1)M_\infty^2}\frac{\partial T}{\partial y}$$

$$q_z = -\frac{\mu}{Pr}\frac{1}{Re}\frac{1}{(\gamma-1)M_\infty^2}\frac{\partial T}{\partial z} \quad T = \frac{\gamma M_\infty^2 p}{\rho}$$

where, Pr, μ and Re are the Prandtl number, dynamic viscosity and Reynolds number respectively. The source terms are given by

$$s_m(\cdot) = \rho\left\{\frac{\partial\cdot}{\partial t} + (\tilde{u}+\hat{u})\frac{\partial\cdot}{\partial x} + (\tilde{v}+\hat{v})\frac{\partial\cdot}{\partial y} + (\tilde{w}+\hat{w})\frac{\partial\cdot}{\partial z}\right\} \tag{9}$$

$$\begin{aligned} s_e(\hat{u},\hat{v},\hat{w}) &= \tilde{u}s_m(\hat{u}) + \tilde{v}s_m(\hat{v}) + \tilde{w}s_m(\hat{w}) + p\left[\frac{\partial\hat{u}}{\partial x} + \frac{\partial\hat{v}}{\partial y} + \frac{\partial\hat{w}}{\partial z}\right] \\ &+ \sigma_{xx}\frac{\partial\hat{u}}{\partial x} + \sigma_{yy}\frac{\partial\hat{v}}{\partial y} + \sigma_{zz}\frac{\partial\hat{w}}{\partial z} + \sigma_{xy}\left[\frac{\partial\hat{v}}{\partial x} + \frac{\partial\hat{u}}{\partial y}\right] + \sigma_{xz}\left[\frac{\partial\hat{w}}{\partial x} + \frac{\partial\hat{u}}{\partial z}\right] + \sigma_{yz}\left[\frac{\partial\hat{w}}{\partial y} + \frac{\partial\hat{v}}{\partial z}\right] \end{aligned} \tag{10}$$

It is noted that the stress tensors, σ, in SVM are calculated based on velocity derivatives for total velocities u, v and w meaning that they include the gust velocities for the calculation of viscous fluxes. This is to eliminate the introduction of dissipative source terms arising from separating velocity derivatives. The resulting equation is the Split Velocity Method equations without any underlying assumptions about the gust. It can be readily seen that this is equivalent to standard moving mesh equations (or FVM) with grid velocity set to minus the gust velocity, but includes additional source terms which are an important aspect of this method as it takes into account all the interactions between the gust and the aircraft.

II.B. Coupling methodology

The flexible aircraft gust encounters were computed using FlowSimulator[13] to couple the CFD solver DLR-TAU, modified to implement SVM, to a structural solver implemented in Python. The FlowSimulator software has been developed to enable multi-disciplinary simulations by providing a common interface for individual computational tools in a plugin-type manner. For this work the CSM solver, CFD solver and deformation tool all interact through this common environment.

This CSM solver uses a modal coupling technique to compute the deformations at each time-step, which reduces the computational cost. The governing differential equation in physical coordinates is given by

$$[M]\{\ddot{u}(t)\} + [D]\{\dot{u}(t)\} + [K]\{u(t)\} = \{f(t)\} \tag{11}$$

where u is the displacement vector, M is the mass matrix, D is the damping matrix, K is the stiffness matrix and f denotes the force vector. The modal form of the governing differential equation for motion is given by multiplying the equation in physical coordinates (11) by the modal matrix, $\Phi = [X_1 X_2 \dots X_N]$ and setting

$$\{u(t)\} = \sum_{r=1}^{N}\{X - r\}\, q_r = [\Phi]\{q(t)\} \tag{12}$$

This gives the governing differential equation for motion as:

$$[\Phi]^T[M][\Phi]\{\ddot{q}(t)\} + [\Phi]^T[D][\Phi]\{\dot{q}(t)\} + [\Phi]^T[K][\Phi]\{q(t)\} = [\Phi]^T\{f(t)\} \tag{13}$$

Where $[\Phi]^T[M][\Phi]$ is the generalized mass matrix, $[\Phi]^T[K][\Phi]$ is the generalized stiffness matrix and q are the generalized coordinates. The force vector, $f(t)$, constitutes the aerodynamic loads, which are calculated using DLR-TAU. The structural displacements calculated by the CSM solver must be interpolated onto the aerodynamic surface points. This is done by linear interpolation given by

$$u_a = [H]u_s \tag{14}$$

where u_a are the displacements at the aerodynamic surface points, u_s are the structural displacements and H is a matrix that gives the coupling between the points of the aerodynamic model and the structural model. This interpolation is performed using an RBF deformation tool. This is a scattered data interpolation method and uses a Wendlands C2 basis function. A conventional serial staggered algorithm[15] is used to couple the fluid system to the structural system, this is a loosely-coupled iterative procedure which means that the accuracy that can be achieved is limited as there will always be a first order error associated with the timestep. The structural equations themselves are integrated in time using the Newmark method.[16]

III. Results

The main requirements driving the investigation of gusts for aircraft are safety and certification. They are set out by the EASA Certification Specification-25 (CS-25) or by the FAR-25 documents. Amendment 12 of CS-25 states that the shape of the gust must be:

$$\hat{v} = \begin{cases} 0 & x < x' - H \qquad x > x' \\ \frac{\hat{v}_{ds}}{2}\left(1 - \cos\left(\frac{\pi(x-x')}{H}\right)\right) & x' \geq x \geq x' - H \end{cases} \tag{15}$$

where x' is the leading-edge position of the gust and is given by

$$x' = u_{ref}t + x_0. \tag{16}$$

Here, u_{ref} is the reference freestream velocity, x_0 is the position of the leading edge of the gust at time zero, H is the gust half-wavelength in metres and $\hat{v}_{ds}$ is the design gust velocity given by:

$$\hat{v}_{ds} = u_{ref}F_g(H/107)^{(1/6)} \tag{17}$$

Where F_g is the flight profile alleviation factor. The value of F_g will be increased linearly from the sea level value to a value of 1 at the maximum operating altitude and can be calculated as directed by CS-25.341. In the equation above, the value 107 refers to the largest half-wavelength (in metres) of importance. The half-wavelengths that are interesting in this study range from 30 ft (9.144m) to 350 ft (106.68m).

Using these equations, the amplitudes were computed using the flight envelope for a generic wide-body aircraft test case. Using the design cruising speed, the gust profiles and flight conditions for the cases simulated are listed in Table 1. These were run on an unstructured mesh, generated in SOLAR,[17] which consisted of a half-model of the wide-body aircraft and contained approximately 3 million points.

The cases were simulated using both the SVM and FVM with the Spalart-Allmaras turbulence model without the ft2 trip term.[18] For all the cases, the gust was initially located outside of the farfield boundary and convected at the freestream velocity speed. All these cases have previously been run rigid and the results were presented by Huntley *et al.*[1] These gusts were chosen as they represent the shortest, mid-length and longest wavelength gust as specified by the Certification Authorities at different flight conditions. The results are presented using a non-dimensional time given by

$$s = \frac{2u_{ref}t}{c} \tag{18}$$

where t is the physical time step size and c is the chord length. This represents the number of semi-chords travelled. A physical time step size of 0.0025s has been used. The results for lift and moment coefficient (normalised by the maximum value) are presented in Figures 1, 2 and 3 for gust simulations at altitudes of 0ft, 29995ft and 43000ft, respectively. All three altitudes show that the Split Velocity Method has a larger effect on shorter wavelength gusts. This is expected as the source terms, which are given by the velocity gradients, are largest here. Figures 1(a), 2(a) and 3(a) show that for the shortest wavelength gusts at each

Table 1. Gust profile data

Altitude (ft)	Mach Number	Reynolds number	Gust length (m)	Gust Velocity (m/s)	Equivalent $\Delta\alpha(deg)$
0	0.499	11×10^6	18.29	8.825	2.98
0	0.499	11×10^6	91.44	11.540	3.89
0	0.499	11×10^6	213.36	13.290	4.48
29995	0.860	8×10^6	18.29	11.247	2.47
29995	0.860	8×10^6	91.44	14.707	3.23
29995	0.860	8×10^6	213.36	16.938	3.72
43000	0.860	5×10^6	18.29	12.692	2.96
43000	0.860	5×10^6	91.44	16.597	3.87
43000	0.860	5×10^6	213.36	19.114	4.45

altitude there are two main peaks in the lift coefficient. The first peak corresponds to the gust passing over the wing whilst the second peak is caused by the gust travelling over the tail of the aircraft.

Pressure coefficient distributions across the surface of the aircraft wing at the time of the gust peak are shown in Figures 4, 5 and 6 for altitudes of 0ft, 29995ft and 43000ft, respectively. The corresponding wing deformations are shown in Figures 7, 8 and 9. From these figures it is clear to see that in the main there is very little difference between the Split Velocity Method and the Field Velocity Method. The largest differences appear to occur for the 91.44m case at an altitude of 29995ft, where the pressure coefficient using FVM is shown in Figure 5(c) and using SVM is shown in Figure 5(d). The corresponding wing deformations are shown in Figure 8(c) with the close-up of the wing tip shown in Figure 8(d). Here it is possible to see that there is greater suction across the upper surface of the wing using FVM which corresponds to a lower deformation at the wing tip. Generally, the results appear to show that for the shortest wavelength gusts there is very little deformation of the wing but the differences between FVM and SVM are greatest here. Whereas for the largest wavelength gusts the deformation is greatest but the difference between FVM and SVM is minimal. This agrees with what was found for the forces and for the rigid cases run previously and presented in Huntley *et al.*[1]

The SVM does incur a cost penalty, this is fairly constant across all the simulations presented here, where the SVM took on average 12.6% longer in terms of CPU time. The number of CPU hours for all cases are given in Table 2. This table also shows the accuracy gain of using the SVM for the global peak values of lift and moment coefficient. This is presented as a negative value if it was found that the FVM overpredicted the peak value and a positive value if FVM underpredicted the peak value. The largest inconsistencies are found with the coefficients of the shortest wavelength gusts. The FVM also tends to overpredict the peak lift coefficient and underpredict the moment coefficient of the shortest wavelength gust. As the gust length increases the differences between SVM and FVM reduce although the peak moment coefficient values show larger differences than the lift coefficient. Furthermore, the peak moment coefficient value seems to be overpredicted by the FVM for the larger wavelength gusts.

Table 2. Computational cost

Altitude (ft)	Gust length (m)	CPU hours		SVM cost (+%)	SVM accuracy improvement (%)	
		FVM	SVM		Cl	Cm
0	18.29	106.8	118.7	11.1	-1.8	-9.5
0	91.44	127.2	145.3	14.2	-0.7	0.3
0	213.36	243.8	274.1	12.4	-0.3	-3.3
29995	18.29	152.0	170.5	12.2	-4.1	11.5
29995	91.44	170.4	194.1	13.9	-1.2	-3.5
29995	213.36	290.4	324.4	11.7	0.2	-1.3
43000	18.29	204.1	227.6	11.5	-3.1	-6.7
43000	91.44	225.6	255.4	13.2	-1.0	-1.0
43000	213.36	340.3	382.5	12.4	0.5	0.5

IV. Conclusion

The Split Velocity Method has been used to investigate the gust response of a flexible aircraft to a series of 1-cosine gusts. This is achieved by coupling the CFD solver DLR-TAU to a modal structural solver to perform aeroelastic calculations. The results were compared to an existing prescribed velocity method currently available in DLR-TAU called the field velocity method. It has been shown that the Split Velocity Method increases the accuracy of simulations of flexible aircraft encounters with short wavelength gusts but has less of an effect for larger wavelength gusts where the gradients are smaller. When considering the gain in accuracy with the increase in computational cost associated with employing the Split Velocity Method, it would suggest that SVM should only be used for the shortest wavelength gusts. The SVM has been shown to convect gusts and disturbances without dissipation while providing far more insight into flow behaviour and generated forces than the widely used linear panel methods. The SVM allows gusts to be resolved and the mutual interaction of the aircraft and the gust to be simulated without requiring a fine mesh to be employed throughout the domain. This allows for detailed modelling at low computational cost thus making it extremely valuable in aircraft design.

Acknowledgments

The research leading to these results was co-funded by Innovate UK, the UKs innovation agency, within the Enhanced Fidelity Transonic Wing project.

References

[1]Huntley, S., Jones, D., and Gaitonde, A., "2D and 3D gust repsonse using a prescribed velocity method," *46th AIAA Fluid Dynamics Conference*, 2016.

[2]Barba, L., Leonard, A., and Allen, C., "Vortex method with meshless spatial adaption for accurate simulation of viscous, unsteady vortical flows," *International Journal for Numerical Methods in Fluids*, Vol. 47, 2005, pp. 841–848.

[3]Wales, C., Gaitonde, A., and Jones, D., "Simulation of airfoil gust rresponse using prescribed velocities," *IFASD*, 2011.

[4]Tang, L. and Baeder, J., "Adaptive euler simulation of supercritical interaction of airfoil and vortex," *AIAA Computational Fluid Dynamics Conference*, 2003.

[5]Tang, L. and Baeder, J., "A two-step grid redistribution method," *Computers & Fluids*, Vol. 32, No. 3, 2003, pp. 323–336.

[6]Parameswaran, V. and Baeder, J., "Indicial aerodynamics in compressible flow-direct computational fluid dynamic calculations," *Journal of Aircraft*, Vol. 34, No. 1, 1997, pp. 131–133.

[7]Singh, R. and Baeder, J., "GeneGeneral moving gust response using CFD with application to airfoil-vortex interaction," *15th Applied Aerodynamics Conference*, 1997.

[8]Singh, R. and Baeder, J., "Direct calculation of three-dimensional Indicial lift response using computational fluid dynamics," *Journal of Aircraft*, Vol. 34, 1997, pp. 465–471.

[9]Sitaraman, J., *CFD based unsteady aerodynamic modeling for rotor aeroelastic analysis*, Ph.D. thesis, University of Maryland, 2003.

[10]Leishman, J., "Subsonic unsteady aerodynamics caused by gusts using the indicial method," *Journal of Aircraft*, 1996.

[11]Heinrich, R. and Reimer, L., "Comparison of different approaches for gust modeling in the CFD code TAU," *International Forum on Aeroelasticity & Structural Dynamics*, 2013.

[12]Wales, C., *Continuation methods for high Reynolds number compressible flows*, Ph.D. thesis, University Of Bristol, 2010.

[13]Meinel, M. and Einarsson, G., "The FlowSimulator framework for massively parallel CFD applications," *Para 2010*, 2010.

[14]Kaiser, C., Friedewald, D., Quero, D., and Nitzsche, J., "Time-linearized analysis of motion-induced and gust-induced airloads with the DLR TAU code," *Deutscher Luft- und Raumfahrtkongess*, 2015.

[15]Farhat, C., van der Zee, K., and Geuzaine, P., "Provably second-order time-accurate loosely-cooupled solution algorithms for transient nonlinear computational aeroelasticity," *Comput. Methods Appl. Mech. Engrg*, Vol. 195, 2006, pp. 1973–2001.

[16]Bathe, K., *Finite Element Procedures in Engineering Analysis*, Prentice Hall, 1982.

[17]Martineau, D., Stokes, S., Munday, S., Jackson, A., Gribben, B., and Verhoeven, N., "Anisotropic hybrid mesh generation for industrial RANS applications," *44th AIAA Aerospace Sciences Meeting and Exhibit*, 2006.

[18]Spalart, P. and Allmaras, S., "A one-equation turbulence model for aerodynamic flows," *AIAA paper*, Vol. 92-0439, 1992.

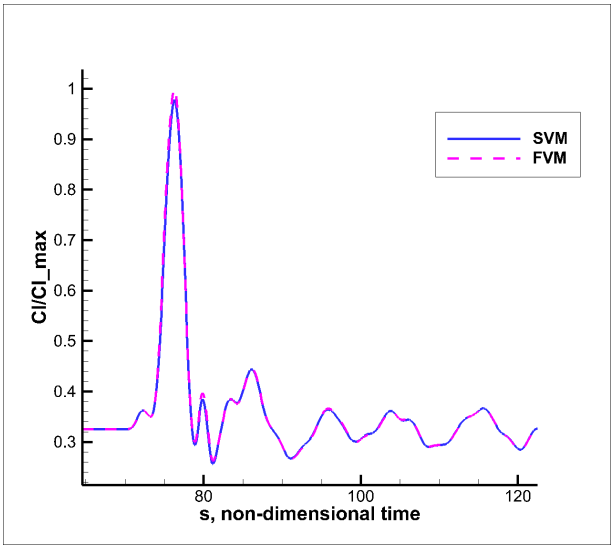

(a) Lift coefficient history an 18.28m wavelength gust

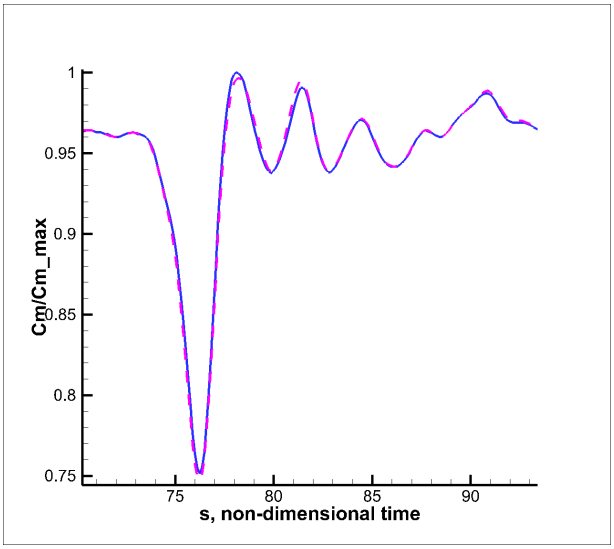

(b) Moment coefficient history an 18.28m wavelength gust

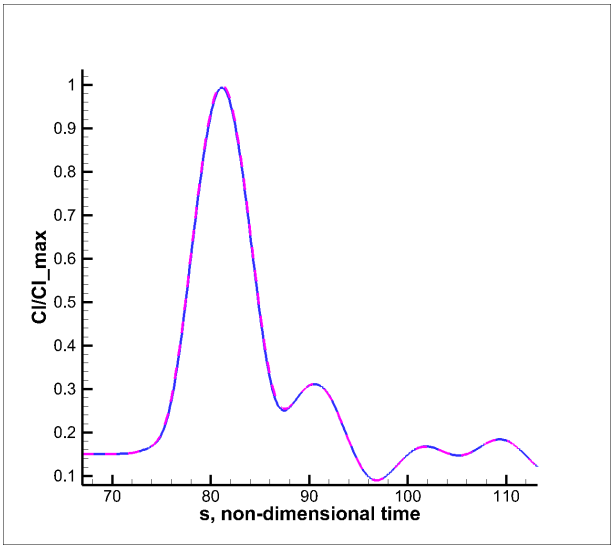

(c) Lift coefficient history an 91.44m wavelength gust

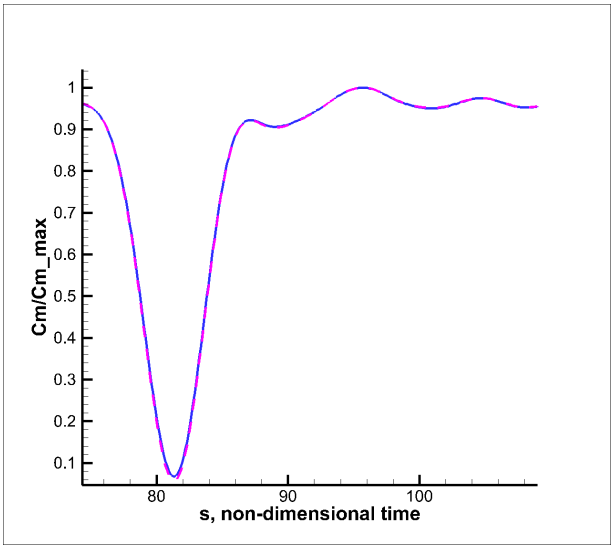

(d) Moment coefficient history an 91.44m wavelength gust

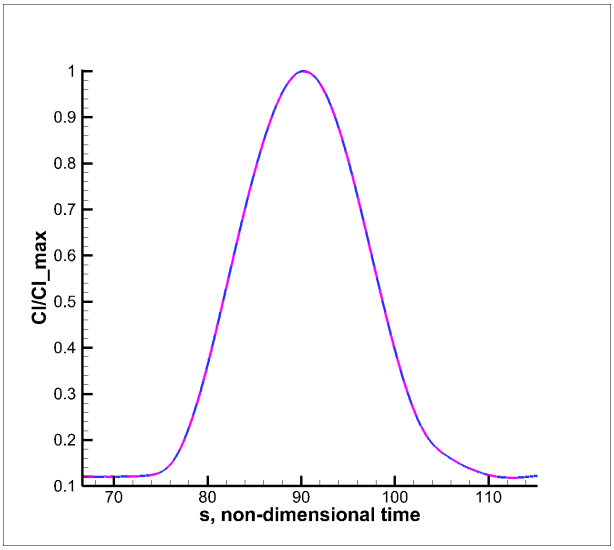

(e) Lift coefficient history an 213.36m wavelength gust

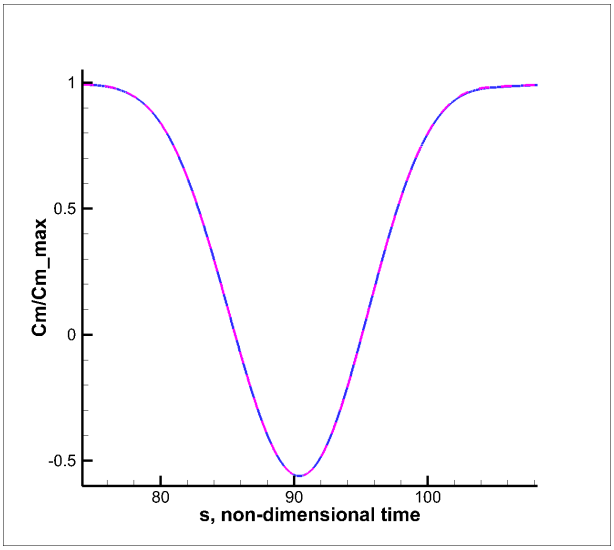

(f) Moment coefficient history an 213.36m wavelength gust

Figure 1. Lift and moment coefficient histories at an altitude of 0ft for different wavelength gusts.

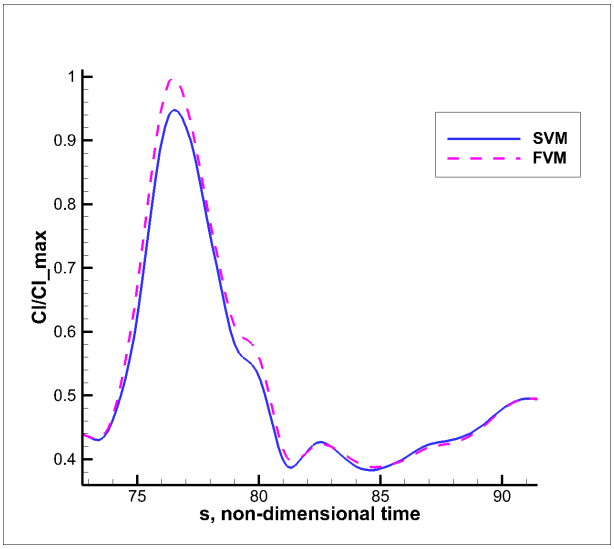

(a) Lift coefficient history an 18.28m wavelength gust

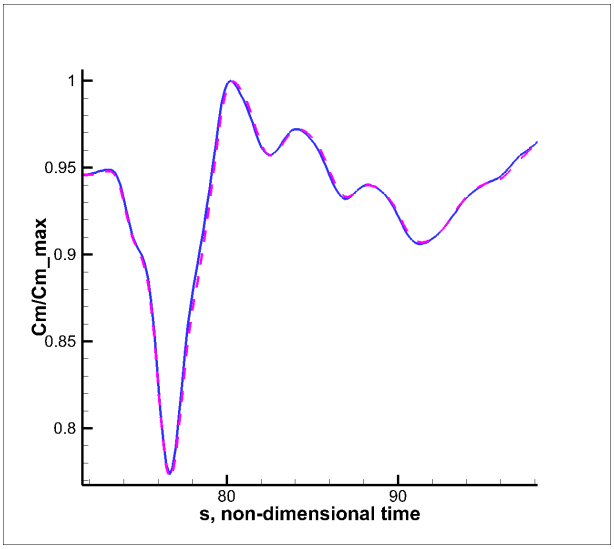

(b) Moment coefficient history an 18.28m wavelength gust

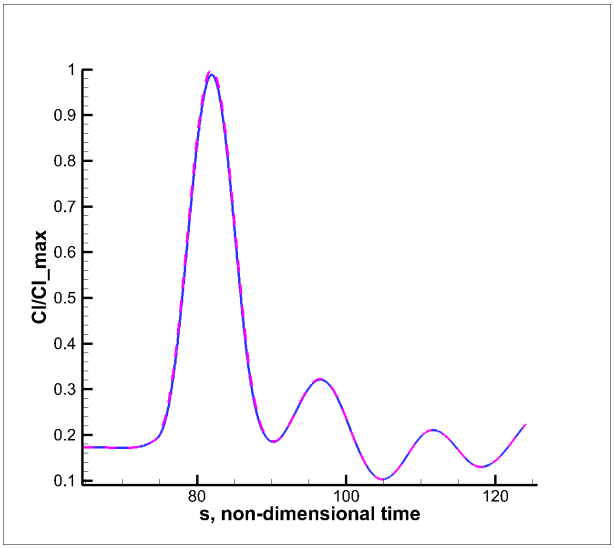

(c) Lift coefficient history an 91.44m wavelength gust

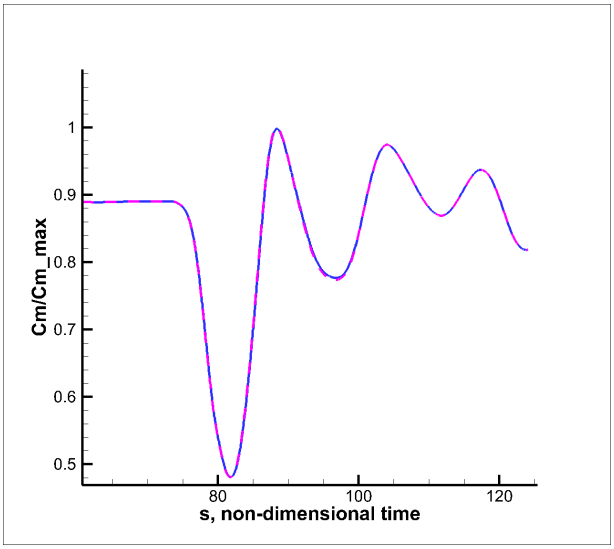

(d) Moment coefficient history an 91.44m wavelength gust

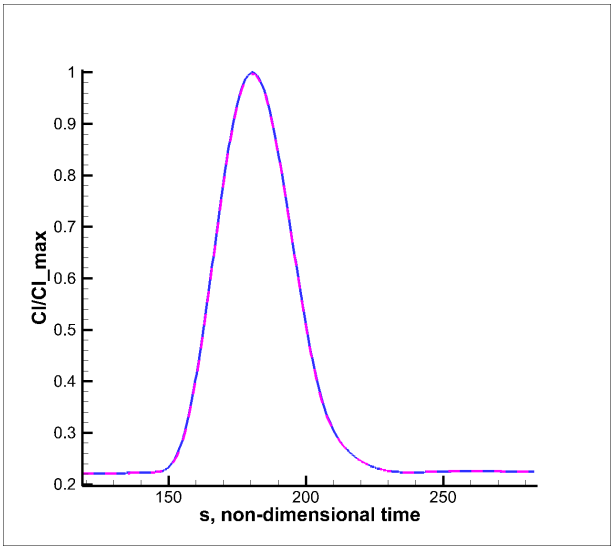

(e) Lift coefficient history an 213.36m wavelength gust

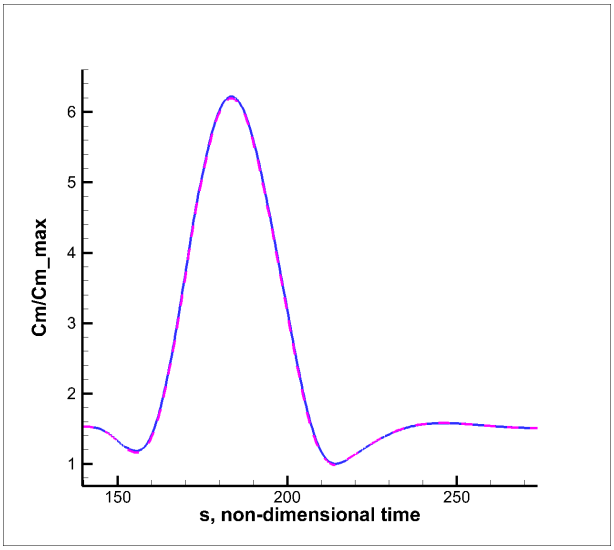

(f) Moment coefficient history an 213.36m wavelength gust

Figure 2. Lift and moment coefficient histories at an altitude of altitude 29995ft for different wavelength gusts.

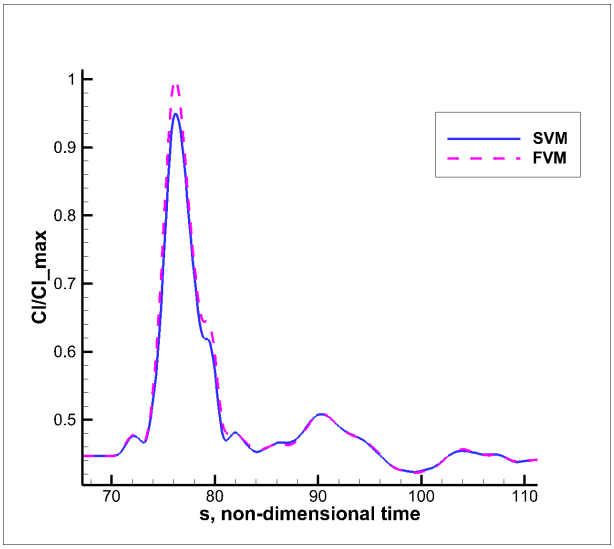

(a) Lift coefficient history an 18.28m wavelength gust

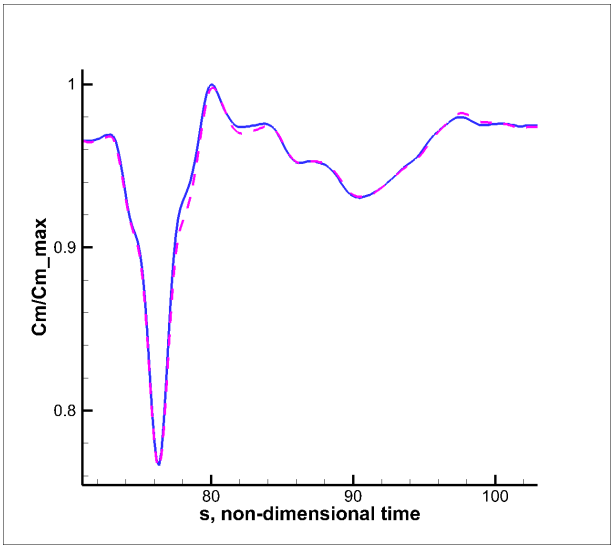

(b) Moment coefficient history an 18.28m wavelength gust

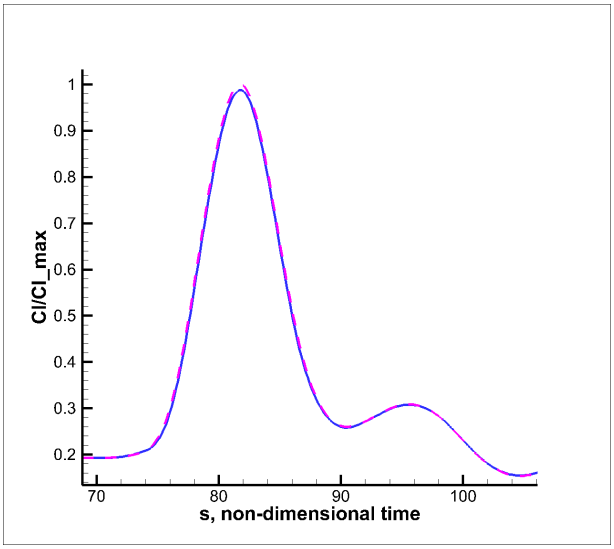

(c) Lift coefficient history an 91.44m wavelength gust

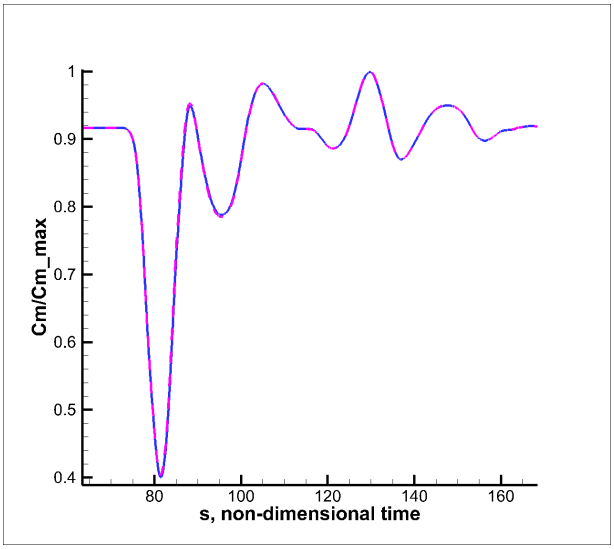

(d) Moment coefficient history an 91.44m wavelength gust

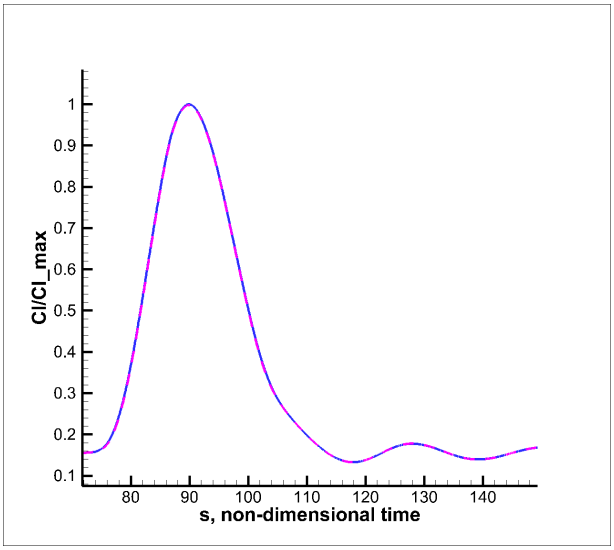

(e) Lift coefficient history an 213.36m wavelength gust

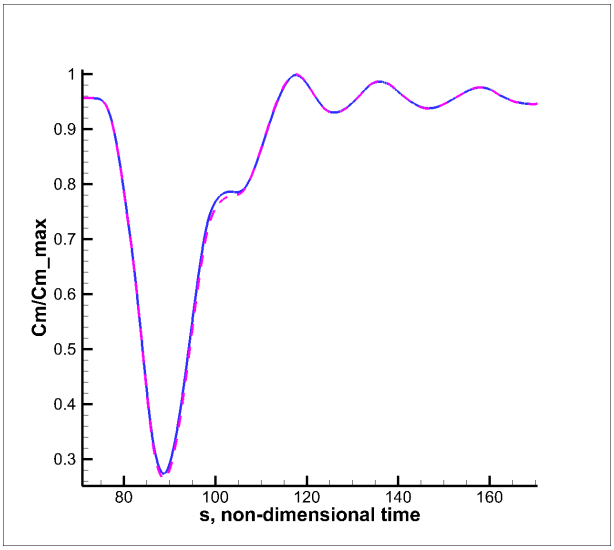

(f) Moment coefficient history an 213.36m wavelength gust

Figure 3. Lift and moment coefficient histories at an altitude of altitude 43000ft for different wavelength gusts.

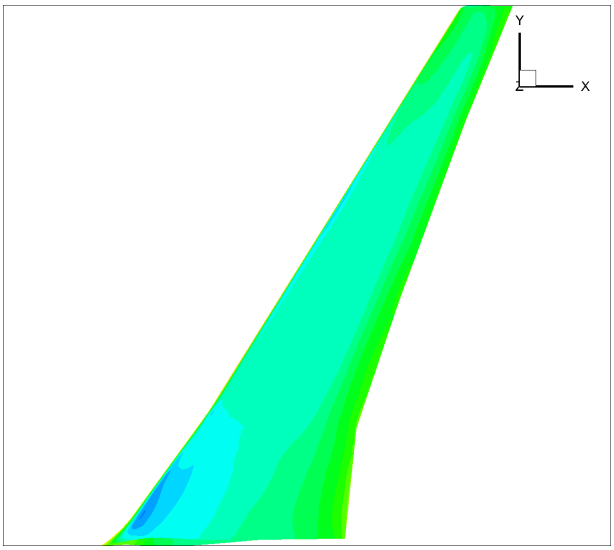

(a) Wing surface Cp of an 18.28m wavelength gust using FVM

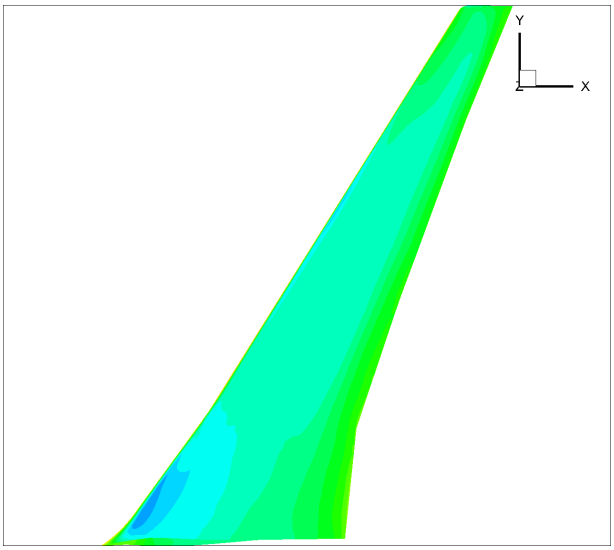

(b) Wing surface Cp of an 18.28m wavelength gust using SVM

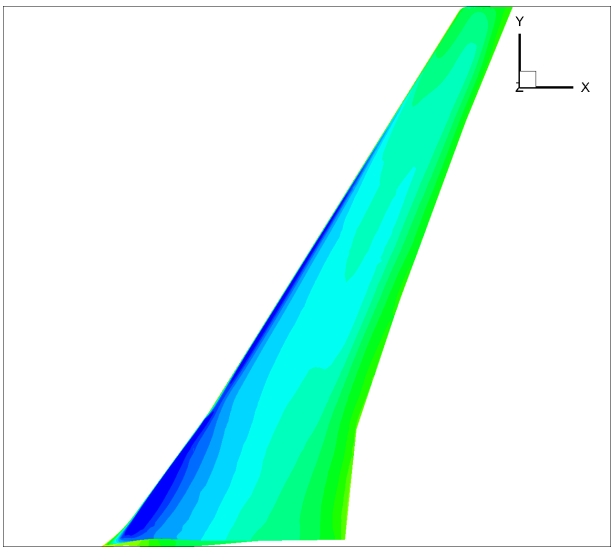

(c) Wing surface Cp of a 91.44m wavelength gust using FVM

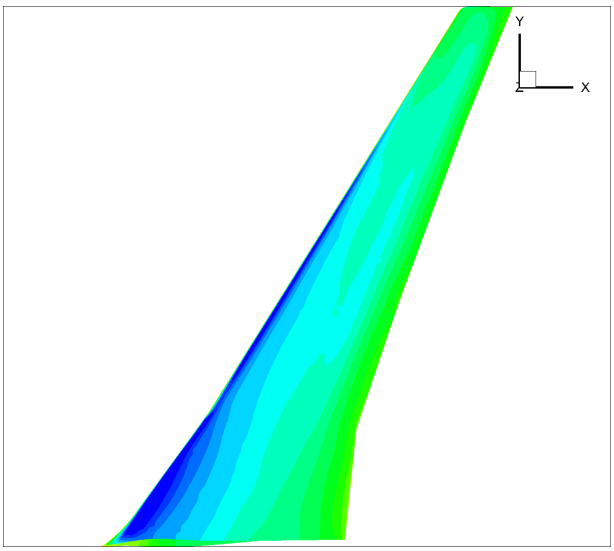

(d) Wing surface Cp of a 91.44m wavelength gust using SVM

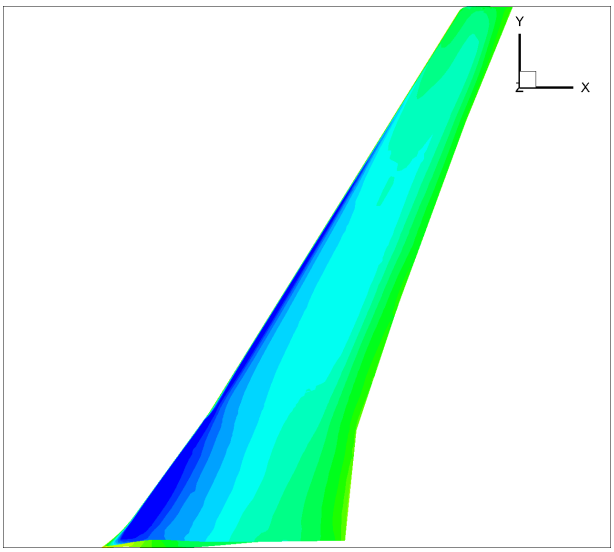

(e) Wing surface Cp of a 213.36m wavelength gust using FVM

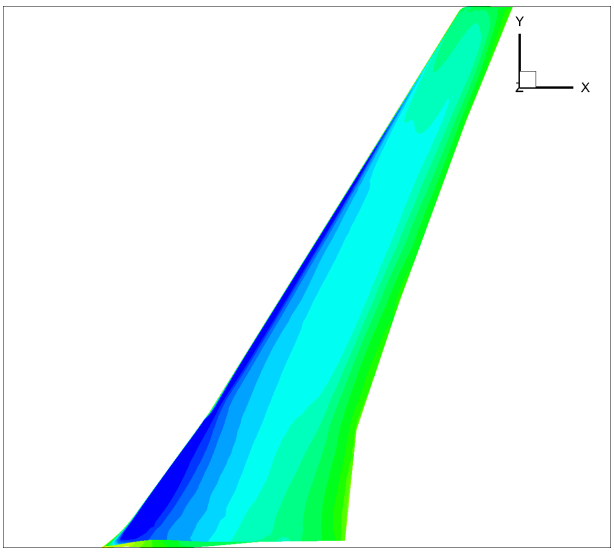

(f) Wing surface Cp of a 213.36m wavelength gust using SVM

Figure 4. Wing pressure coefficient at gust peak at an altitude of 0ft for different wavelength gusts using SVM and FVM.

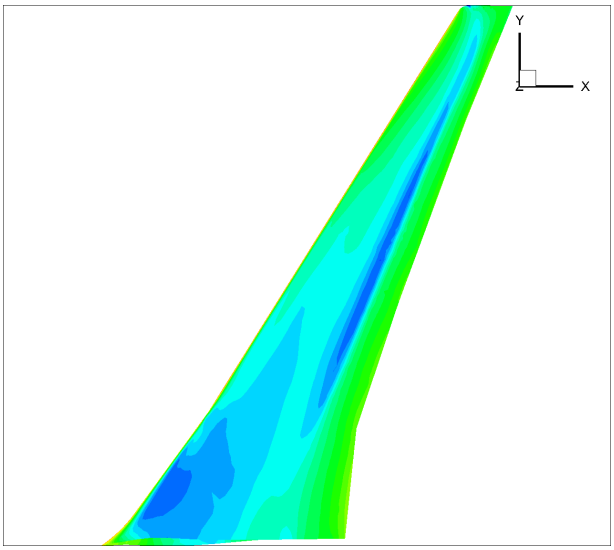

(a) Wing surface Cp of an 18.28m wavelength gust using FVM

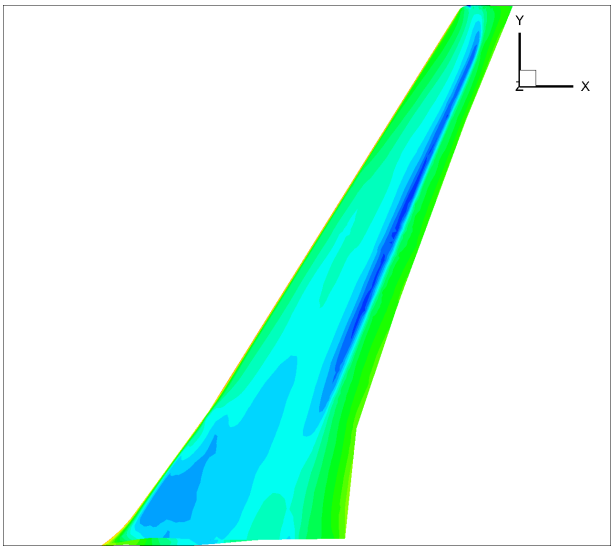

(b) Wing surface Cp of an 18.28m wavelength gust using SVM

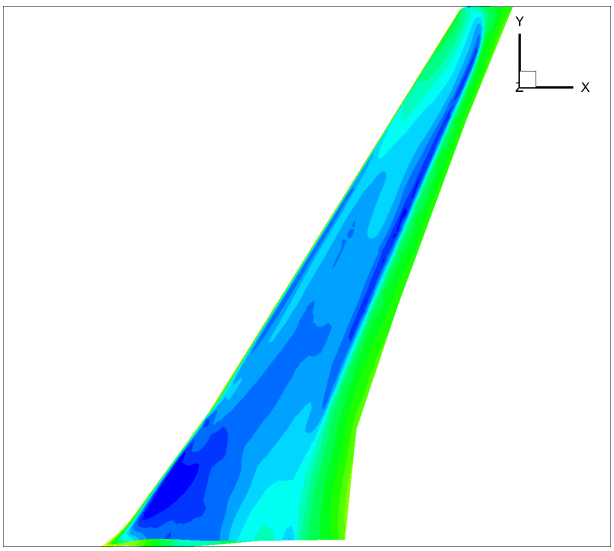

(c) Wing surface Cp of a 91.44m wavelength gust using FVM

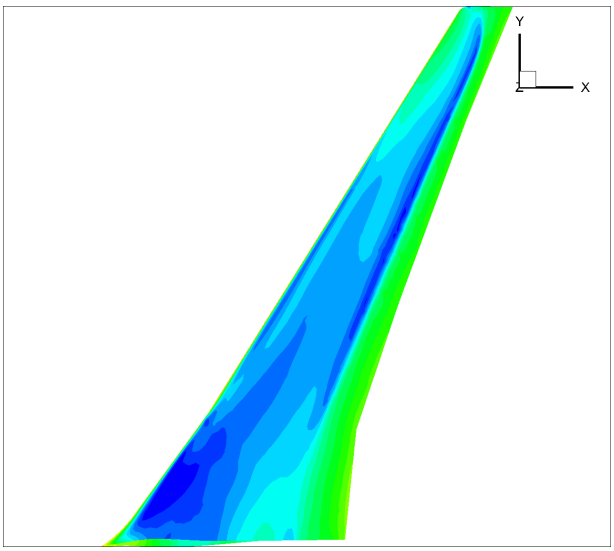

(d) Wing surface Cp of a 91.44m wavelength gust using SVM

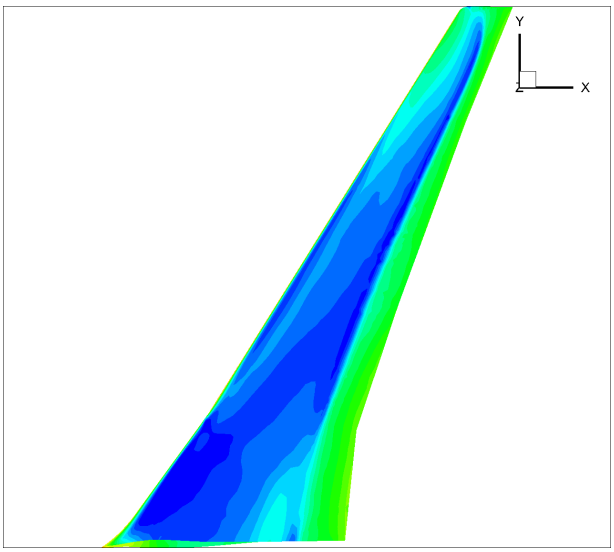

(e) Wing surface Cp of a 213.36m wavelength gust using FVM

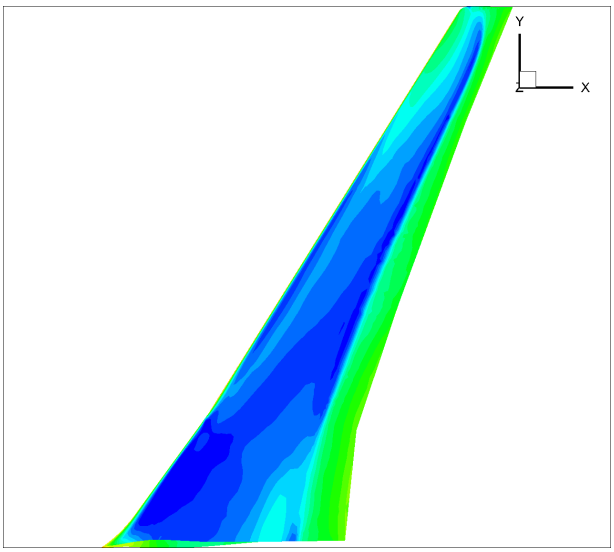

(f) Wing surface Cp of a 213.36m wavelength gust using SVM

Figure 5. Wing pressure coefficient at gust peak at an altitude of 29995ft for different wavelength gusts using SVM and FVM.

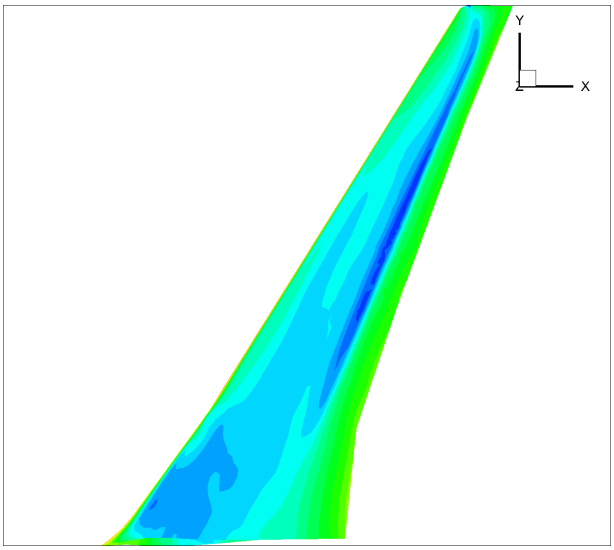

(a) Wing surface Cp of an 18.28m wavelength gust using FVM

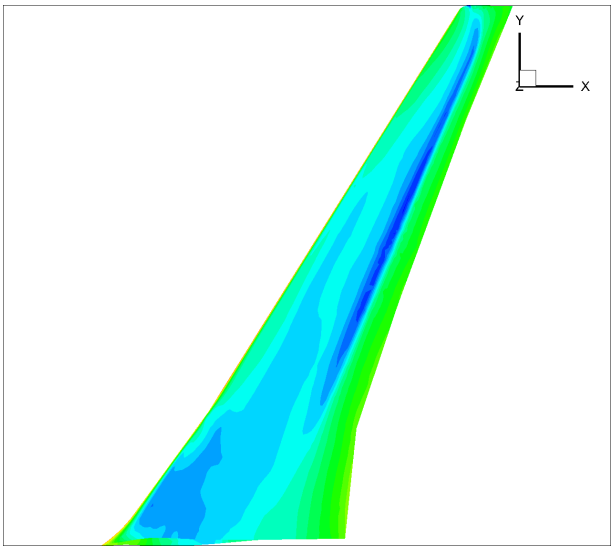

(b) Wing surface Cp of an 18.28m wavelength gust using SVM

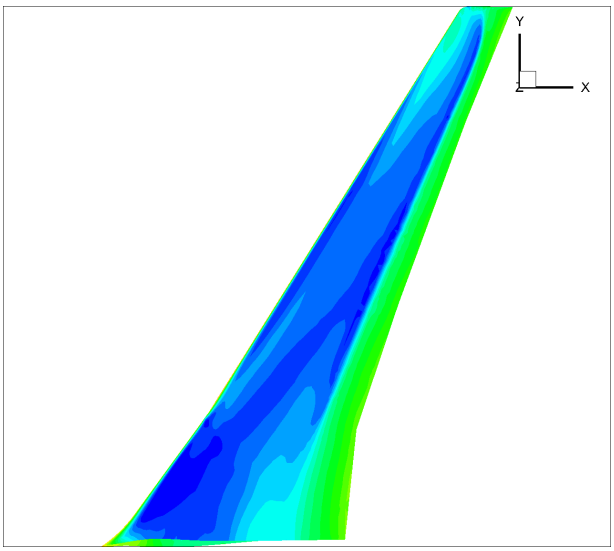

(c) Wing surface Cp of a 91.44m wavelength gust using FVM

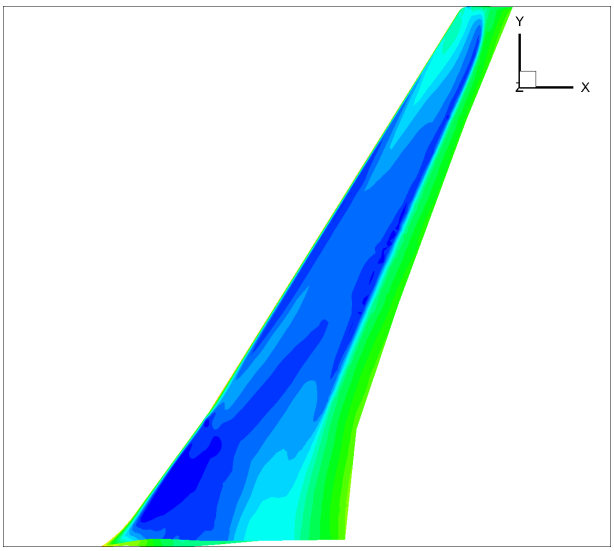

(d) Wing surface Cp of a 91.44m wavelength gust using SVM

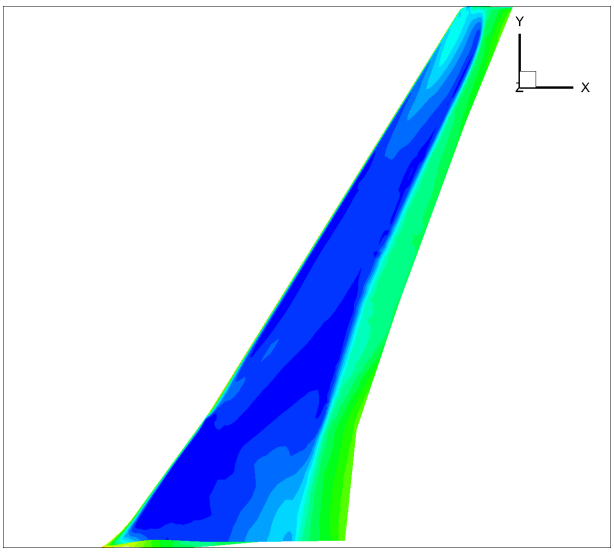

(e) Wing surface Cp of a 213.36m wavelength gust using FVM

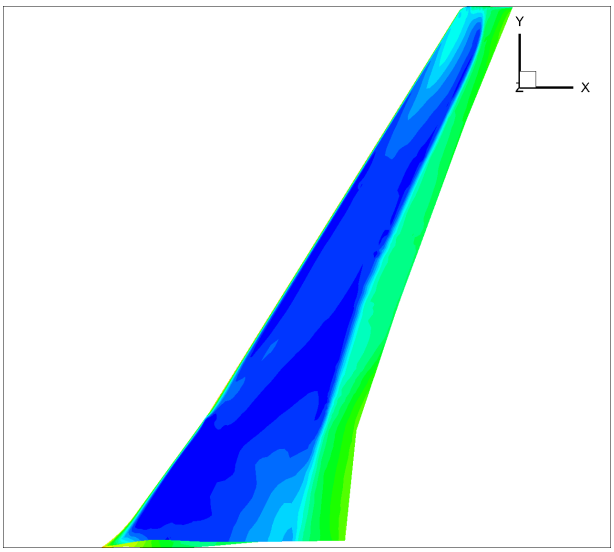

(f) Wing surface Cp of a 213.36m wavelength gust using SVM

Figure 6. Wing pressure coefficient at gust peak at an altitude of 43000ft for different wavelength gusts using SVM and FVM.

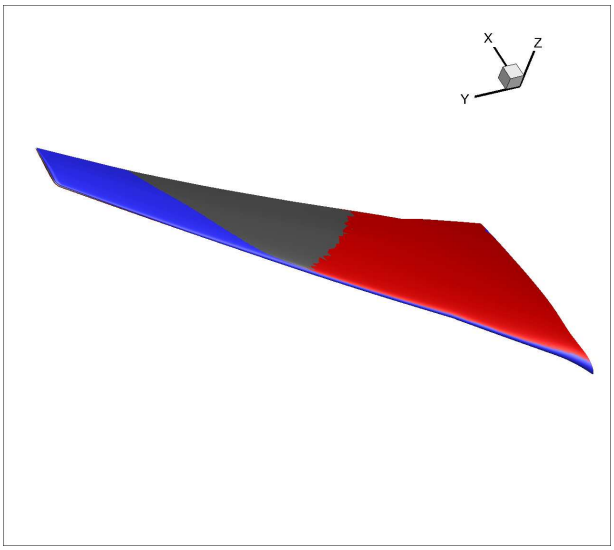

(a) Wing deformation of an 18.28m wavelength gust

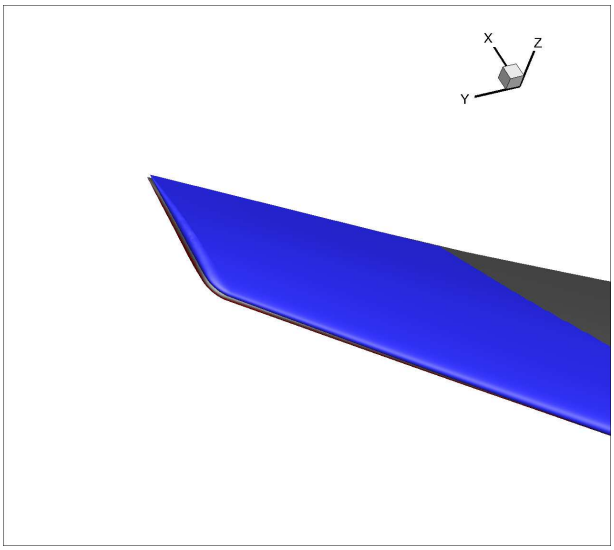

(b) Close up of deformation of an 18.28m wavelength gust

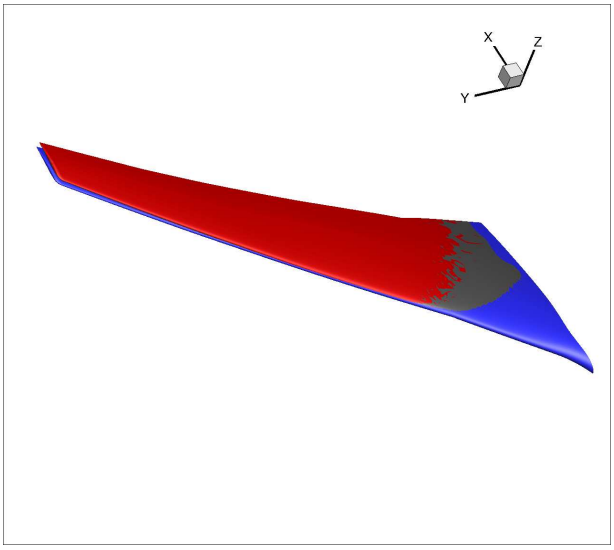

(c) Wing deformation of a 91.44m wavelength gust

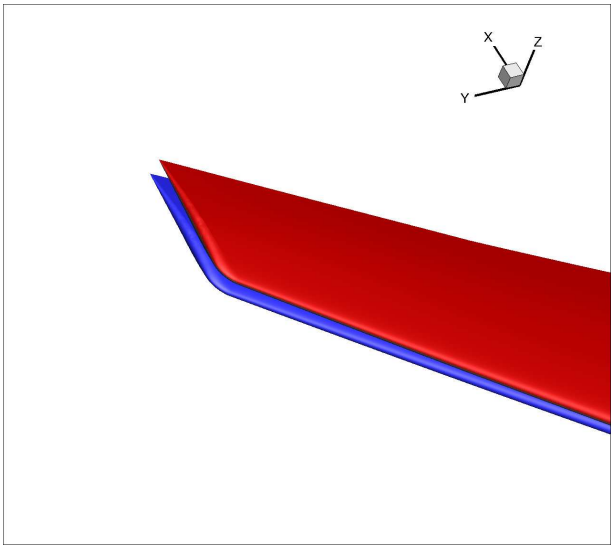

(d) Close up of deformation of a 91.44m wavelength gust

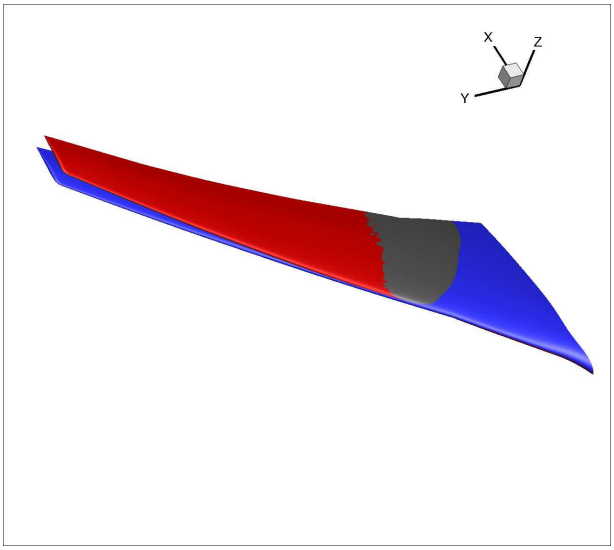

(e) Wing deformation of a 213.36m wavelength gust

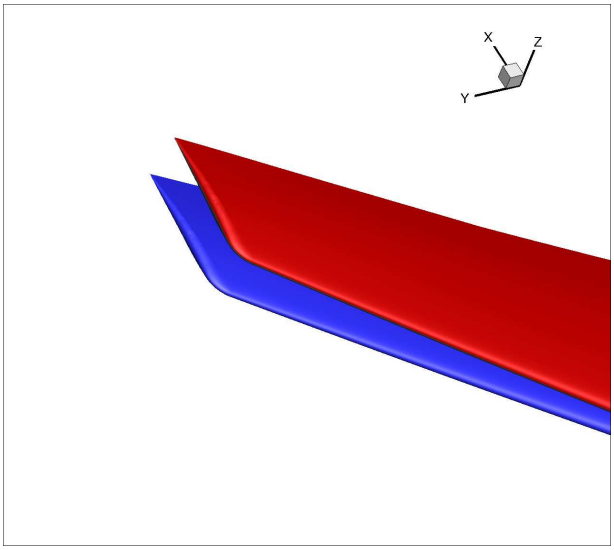

(f) Close up of deformation of a 213.36m wavelength gust

Figure 7. Deformation of at gust peak at an altitude of 0ft for different wavelength gusts. Blue: Initial mesh, Red: FVM, Grey: SVM.

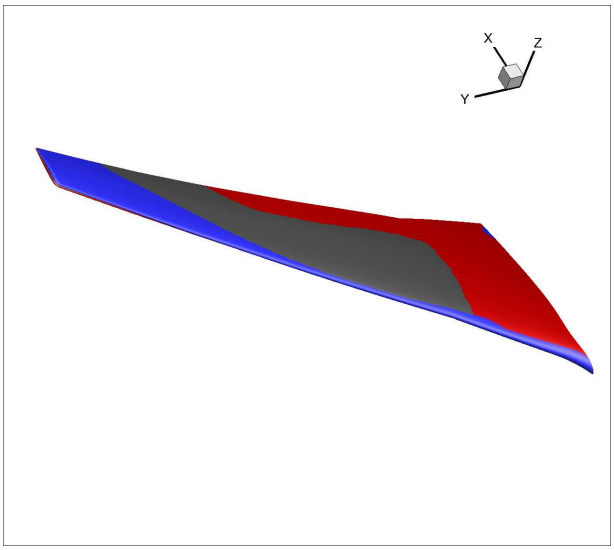

(a) Wing deformation of an 18.28m wavelength gust

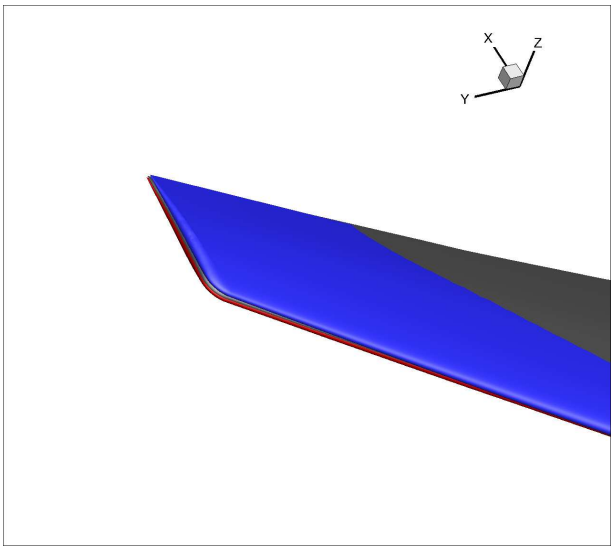

(b) Close up of deformation of an 18.28m wavelength gust

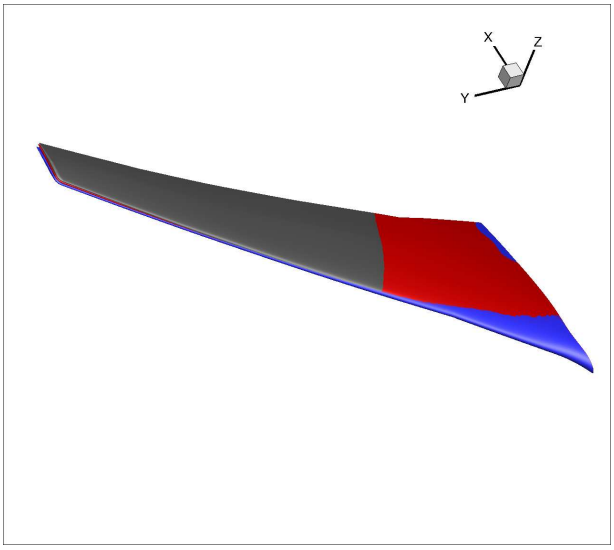

(c) Wing deformation of a 91.44m wavelength gust

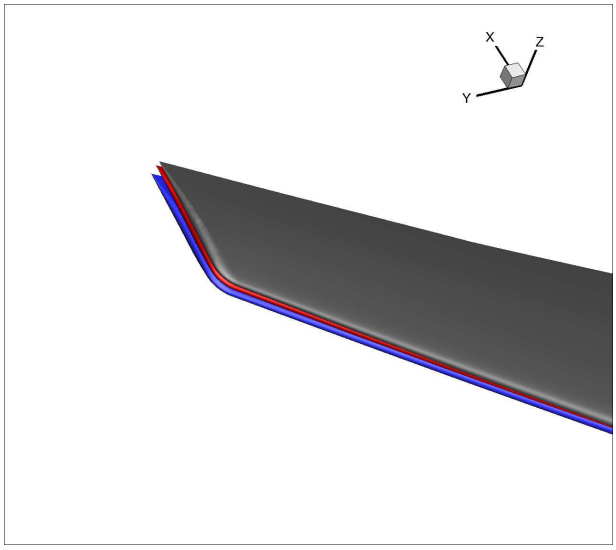

(d) Close up of deformation of a 91.44m wavelength gust

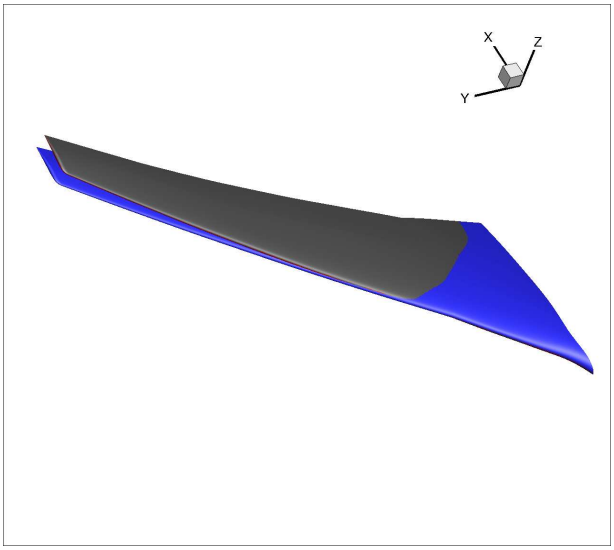

(e) Wing deformation of a 213.36m wavelength gust

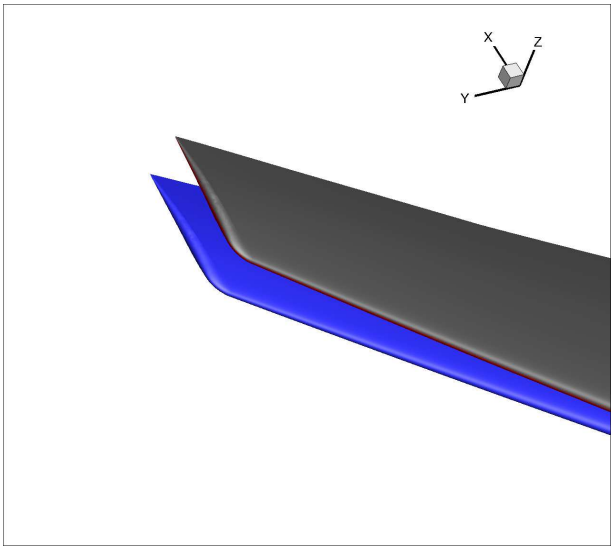

(f) Close up of deformation of a 213.36m wavelength gust

Figure 8. Deformation of at gust peak at an altitude of 29995ft for different wavelength gusts. Blue: Initial mesh, Red: FVM, Grey: SVM.

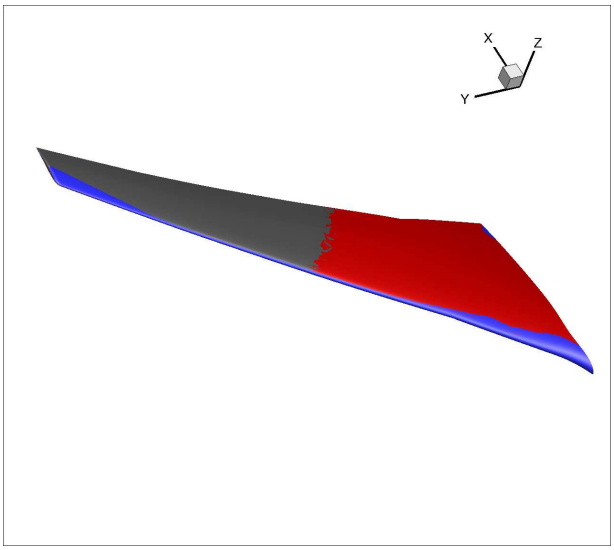

(a) Wing deformation of an 18.28m wavelength gust

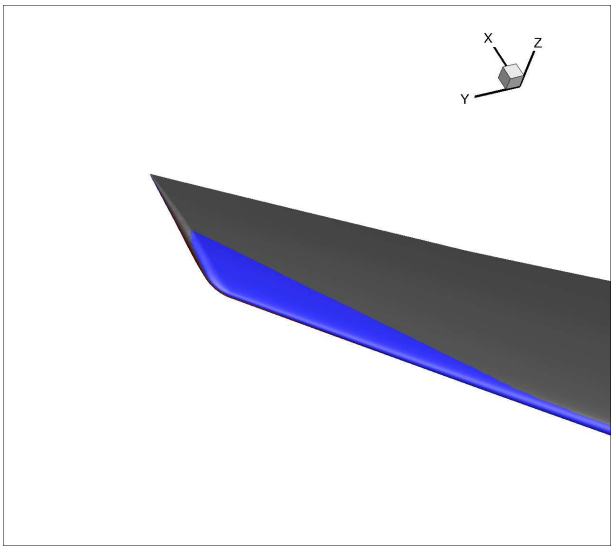

(b) Close up of deformation of an 18.28m wavelength gust

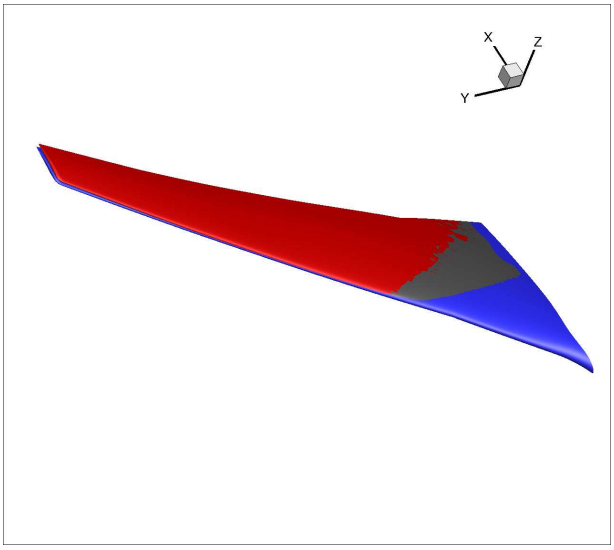

(c) Wing deformation of a 91.44m wavelength gust

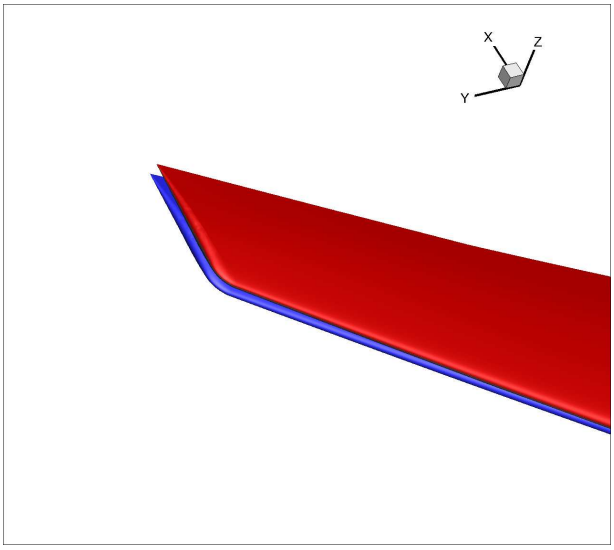

(d) Close up of deformation of a 91.44m wavelength gust

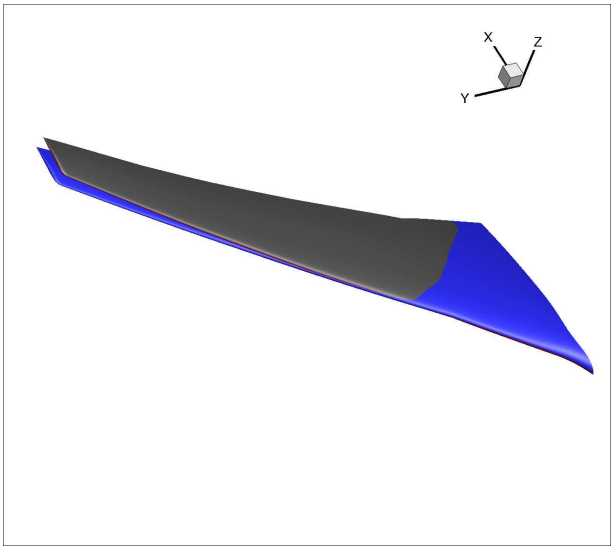

(e) Wing deformation of a 213.36m wavelength gust

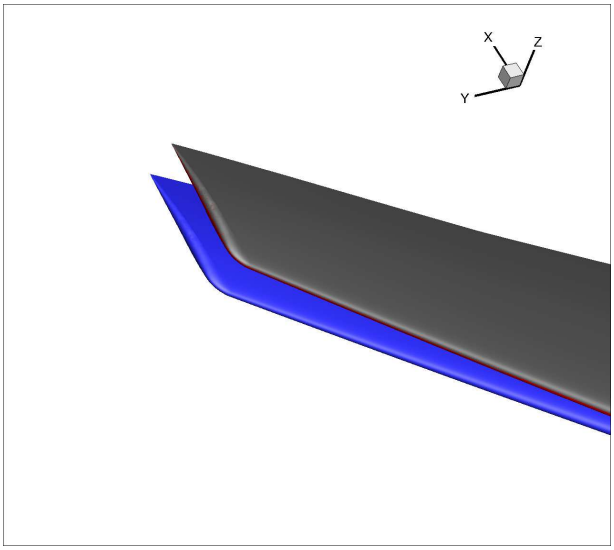

(f) Close up of deformation of a 213.36m wavelength gust

Figure 9. Deformation of at gust peak at an altitude of 43000ft for different wavelength gusts. Blue: Initial mesh, Red: FVM, Grey: SVM.